IEEE Access
Multidisciplinary | Rapid Review | Open Access Journal

Received May 23, 2022, accepted June 7, 2022, date of publication June 15, 2022, date of current version June 21, 2022.

Digital Object Identifier 10.1109/ACCESS.2022.3183209

Distributed Control and Optimization of DC Microgrids: A Port-Hamiltonian Approach

BABAK ABDOLMALEKI, (Member, IEEE), AND GILBERT BERGNA-DIAZ, (Member, IEEE)
Department of Electric Power Engineering, Norwegian University of Science and Technology, 7491 Trondheim, Norway

Corresponding author: Babak Abdolmaleki (babak.abdolmaleki@ntnu.no)

This work was supported by the Department of Electric Power Engineering, Norwegian University of Science and Technology.

ABSTRACT This article proposes a distributed secondary control scheme that drives a dc microgrid to an equilibrium point where the generators share optimal currents, and their voltages have a weighted average of nominal value. The scheme does not rely on the electric system topology nor its specifications; it guarantees plug-and-play design and functionality of the generators. First, the incremental model of the microgrid system with constant impedance, current, and power devices is shown to admit a port-Hamiltonian (pH) representation, and its passive output is determined. The economic dispatch problem is then solved by the Lagrange multipliers method; the Karush-Kuhn-Tucker conditions and weighted-average formation of voltages are then formulated as the control objectives. We propose a control scheme that is based on the Control by Interconnection design philosophy, where the consensus-based controller is viewed as a virtual pH system to be interconnected with the physical one. We prove the regional asymptotic stability of the closed-loop system using Lyapunov and LaSalle theorems. Equilibrium analysis is also conducted based on the concepts of graph theory and economic dispatch. Finally, the effectiveness of the presented scheme for different case studies is validated with a test microgrid system, simulated in both MATLAB/Simulink and OPAL-RT environments.

INDEX TERMS Control by interconnection, economic dispatch, dc microgrid, distributed control, port Hamiltonian modeling, secondary control.

I. INTRODUCTION

Electric power systems are shifting towards the use of more green technologies. To effectively integrate the renewable energy resources, energy storage systems, and electric loads into the power systems, they are interfaced with the grid via power electronic converters and are grouped in the form of microgrids (MGs) easing their control and management [1], [2]. As a key component of modern power systems, dc microgrids have recently become more attractive [3]. They are compatible with the dc electric nature of renewable energy resources, energy storage systems, and a majority of electric loads. In addition, compared to ac MGs where control of frequency, phase, reactive power, and power quality are big challenges, control and management of dc grids are inherently simpler [3].

In dc MGs, distributed generators (DGs) and loads are connected to the grid via power converters which are either *voltage-controlled* (*grid-forming*) or *current/power-controlled* (*grid-following*). Grid-forming devices adjust the voltage of their point of common coupling (PCC) to follow a given voltage reference. The grid-following devices, on the other hand, follow some current/power references [4]. Therefore, in terms of current/power, the grid-forming DGs and loads are *dispatchable* while the grid-following ones are *non-dispatchable* and can be considered as constant current/power loads. In autonomous MGs, normally a cluster of dispatchable (grid-forming) generators are in charge of shaping the desired voltage level; thus, they should control the dc MG in a collaborative effort.

A common practice to dispatch the current and to adjust the voltage of grid-forming DGs in a decentralized, communication-free fashion is *droop control*. Despite its simple and robust functionality, this primary controller cannot guarantee desired current-sharing and voltage formation between the DGs [5]. To address these shortcomings, the droop characteristic can be corrected by a secondary controller. A secondary control is an upper-level controller which

The associate editor coordinating the review of this manuscript and approving it for publication was Francesco Tedesco.

is usually applied to the system to compensate for the deficiencies of the primary controllers such as inaccurate current-sharing [5]. This controller exploits data exchange either between the DGs and a central control unit or only between the DGs. In the former case, the controller is known as *centralized* secondary control which exhibits a single-point-of-failure to the system and requires a complex communication network between the DGs and the central control unit. Therefore, the distributed control techniques, using neighbor-to-neighbor inter-DG data transmissions, are preferred to the centralized ones [6].

A. EXISTING LITERATURE AND RESEARCH GAP

Distributed control of dc MGs has already been addressed in many works. A consensus-based proportional current-sharing strategy is proposed in [7] where a dynamic consensus-based estimator is additionally employed to keep the average voltage at nominal value. To reduce the communication burden and to reach faster convergence under this controller, it has respectively been modified to event-triggered and finite-time versions in [8] and [9]. In [10] and [11], some distributed optimal control schemes are proposed under which the DGs can achieve economic current-sharing. In [11], to overcome the initialization and noise robustness problems related to dynamic consensus-based estimation, a modified dynamic consensus-based average voltage observer is used which determines the voltage reference of converters so that the DG currents are shared properly. A somewhat similar control strategy to [7], but with event-triggered communications, is proposed in [12] under which only information of the DGs' currents are communicated among them. In [13], a distributed nonlinear controller is proposed for dc MGs which, instead of droop controller, tunes the DGs voltages so their currents are shared proportionally. To bound the DG voltages within a reasonable range and to guarantee current-sharing among them *to a certain degree*, in [14], a containment-consensus-based controller is proposed for dc MGs. A very similar containment-based controller, but with finite-time convergence, is also proposed in [15]. In the above mentioned works, either the electric network dynamics and electrical system are not taken into account or only a simplified linear algebraic representation of the grid is considered. Consequently, the controller design and system stability may depend on the parameters of the physical system which are subject to modelling uncertainties.

One way to achieve plug-and-play (PnP) design and operation is to consider the overall system dynamics and to control the system based on energy principles. To do so, in [16], a distributed passivity-based control is proposed for buck-converter-based MGs ensuring proportional current-sharing and average voltage regulation among the DGs. Some similar versions of this controller are presented in [17]–[19] which demonstrate superior transient system performance. It should be noted that the asymptotic stochastic stability of the controller proposed in [19] has further been studied in [20] under varying loads. To reach the desired control objectives in the mentioned works in a finite-time manner, some sliding mode controllers have been developed in [21], [22]. Moreover, a few consensus-based proportional current-sharing and voltage-balancing controllers, facilitating PnP operations, have been proposed in [23] and [24] for dc MGs with constant power and exponential loads where the existence and stability of the system equilibria is also studied. Following the same concept and for the sake of PnP functionality of the DGs, in [25], a distributed dynamic control strategy is proposed for voltage balancing and proportional current-sharing among parallel buck converters with the same capacity. The aforementioned works are, however, limited to buck converter-based DGs and *proportional current-sharing* and none of them has considered droop-controlled DGs and their *economic current dispatch*.

B. CONTRIBUTIONS

Motivated by the above literature review, a distributed secondary control strategy for dc MGs with ZIP loads is proposed herein with the following noticeable features. First, in the modeling of the power system, the dynamics of transmission lines and shunt capacitors are considered, loads and also current/power-controlled DGs are modeled by constant-impedance-current-power (ZIP) loads, and the generators are characterized by droop-based grid-forming DGs, encompassing various types of interfacing converters. It is shown that the incremental model of the droop-based MG admits a port-Hamiltonian (pH) representation [26], and its passive output is defined. In other words, the MG system can be considered as a port-Hamiltonian multi-agent system [27], [28]. Second, drawing inspiration from the Control by Interconnection (CbI) technique of pH systems [29], a distributed consensus-based secondary controller is proposed which drives the MG to an equilibrium point where *i)* the DGs share optimal currents, and *ii)* their weighted-average voltage is the nominal voltage. The weights applied to the voltages are directly related to coefficients of the DGs cost functions and not the electric network and loads. Third, regional asymptotic stability of the system with ZIP loads is demonstrated and it is shown that the system is globally asymptotically stable without the presence of constant power loads (CPLs). Finally, equilibrium analysis is conducted based on the concepts of economic dispatch and graph theory.

The rest of this paper is structured as follows. The MG system modeling and the control aims are formulated in Section II. Section III presents the proposed controller and the system stability and equilibrium analyses. The case studies and simulation results are given in Section IV. Finally, Section V concludes the paper and discusses future works.

C. NOTATION

Throughout the paper, $\mathbb{R}^{n\times m}$ and $\mathbb{R}^n$ stand for the set of $n \times m$ real matrices and $n \times 1$ real vectors, respectively. $\text{diag}\{x_i\}$ indicates a diagonal matrix with x_i being the corresponding diagonal arrays. $\text{col}\{x_i\}$ shows a column vector with the arrays x_i. $\mathcal{I}$ is an identity matrix with appropriate dimensions. $\mathbf{0}$ and

1 are appropriate all-one and all-zero vectors or matrices. The transpose of a matrix/vector $\mathbf{z}$ is given by $\mathbf{z}^\top$. Given the scalar x or the vector $\mathbf{x}$, $\bar{x}$ and $\bar{\mathbf{x}}$ are their value at the equilibrium point, and $\tilde{x} = x - \bar{x}$ and $\tilde{\mathbf{x}} = \mathbf{x} - \bar{\mathbf{x}}$ their associated incremental variables.

II. MICROGRID MODELING AND CONTROL OBJECTIVES

A. ELECTRIC NETWORK, GENERATORS, AND ZIP LOAD MODELS

Let $\mathcal{N}_e$, $\mathcal{E}_e$, and $\mathcal{G}_e$, with the cardinalities $n_e^{\mathcal{N}}$, $n_e^{\mathcal{E}}$, and $n_e^{\mathcal{G}}$, be the sets of buses, transmission lines, and grid-forming (voltage-controlled) generators, respectively. Suppose that the transmission lines are modeled by serial resistor-inductor pairs, the buses are modeled by shunt capacitors and ZIP loads, and each generator is modeled by a controllable voltage source which is connected to the grid via a transmission line (See Fig. 1).

The described electric network can be modeled as two graphs $\mathcal{M}_e$ and $\mathcal{M}_e^{\mathcal{G}}$ where the buses and transmission lines play the roles of their nodes and edges, respectively. Consider the graph $\mathcal{M}_e = (\mathcal{N}_e, \mathcal{E}_e, \mathcal{B}_e)$ where $\mathcal{N}_e = \{1, \cdots, n_e^{\mathcal{N}}\}$, $\mathcal{E}_e = \{1, \cdots, n_e^{\mathcal{E}}\}$, and $\mathcal{B}_e = [b_{kj}] \in \mathbb{R}^{n_e^{\mathcal{N}} \times n_e^{\mathcal{E}}}$ are its node set, edge set, and incidence matrix, respectively. Similarly, the graph $\mathcal{M}_e^{\mathcal{G}} = (\mathcal{N}_e, \mathcal{G}_e, \mathcal{B}_e^{\mathcal{G}})$ can be defined with the same node set but different edge set $\mathcal{G}_e = \{1, \cdots, n_e^{\mathcal{G}}\}$ and incidence matrix $\mathcal{B}_e^{\mathcal{G}} = [b_{ki}^{\mathcal{G}_e}] \in \mathbb{R}^{n_e^{\mathcal{N}} \times n_e^{\mathcal{G}}}$. An *incidence matrix* describes the network graph topology by determining the connections between the bus voltages and line currents. For the electric network, one should first consider an *arbitrary* current-flow direction for every line (edge); if current of jth line enters node k then $b_{kj} = 1$, if it leaves node k then $b_{kj} = -1$, otherwise $b_{kj} = 0$. Similarly, if ith DG injects current to bus k via an output connector, then $b_{ki}^{\mathcal{G}_e} = 1$; otherwise, $b_{ki}^{\mathcal{G}_e} = 0$. Note that in this work, the generators are assumed to only inject current to the loads and network and not to absorb it, i.e., $b_{ki}^{\mathcal{G}_e} = -1$ is not considered.

According to Fig. 1 and based on the system incidence matrices, the dynamics of the droop-based microgrid system are as follows.

$$L_i^{\mathcal{G}_e} \dot{I}_i^{\mathcal{G}_e} = V_i - \sum\nolimits_k b_{ki}^{\mathcal{G}_e} V_k^{\mathcal{N}_e} - R_i^{\mathcal{G}_e} I_i^{\mathcal{G}_e}, \tag{1a}$$

$$L_j^{\mathcal{E}_e} \dot{I}_j^{\mathcal{E}_e} = -\sum\nolimits_k b_{kj} V_k^{\mathcal{N}_e} - R_j^{\mathcal{E}_e} I_j^{\mathcal{E}_e}, \tag{1b}$$

$$C_k^{\mathcal{N}_e} \dot{V}_k^{\mathcal{N}_e} = \sum\nolimits_j b_{kj} I_j^{\mathcal{E}_e} + \sum\nolimits_i b_{ki}^{\mathcal{G}_e} I_i^{\mathcal{G}_e} - I_k^{\mathrm{L}}, \tag{1c}$$

$$I_k^{\mathrm{L}} = G_k^{\mathrm{cte}} V_k^{\mathcal{N}_e} + I_k^{\mathrm{cte}} + P_k^{\mathrm{cte}} / V_k^{\mathcal{N}_e}, \tag{1d}$$

$$V_i = V_i^{\mathrm{ref}} = V_{\mathrm{nom}} - R_i^D I_i^{\mathcal{G}_e} + u_i, \tag{1e}$$

where $L_i^{\mathcal{G}_e}$, $R_i^{\mathcal{G}_e}$, and $I_i^{\mathcal{G}_e}$, $\forall i \in \mathcal{G}_e$ are inductance, resistance, and current of ith generator transmission line; $L_j^{\mathcal{E}_e}$, $R_j^{\mathcal{E}_e}$, and $I_j^{\mathcal{E}_e}$, $\forall j \in \mathcal{E}_e$ are jth line inductance, resistance, and current; $C_k^{\mathcal{N}_e}$, I_k^{L}, and $V_k^{\mathcal{N}_e}$, $\forall k \in \mathcal{N}_e$ are capacitance, load current, and voltage at bus k; $G_k^{\mathrm{cte}} \geq 0$, I_k^{cte}, and P_k^{cte} are respectively constant conductance, current, and power values of the ZIP load at bus k; V_{nom}, V_i, and V_i^{ref} are nominal voltage and ith DG voltage and its reference value, respectively; R_i^D and u_i are respectively the droop coefficient and correction term (input) of ith generator.

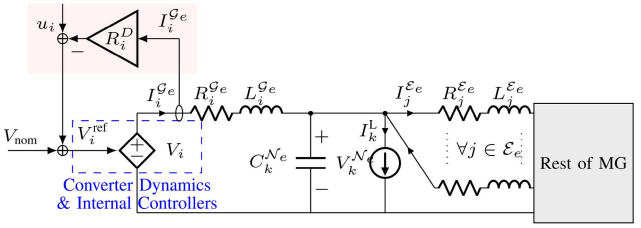

FIGURE 1. A droop-based DG connected to a microgrid with ZIP load.

There are various types of internal current and/or voltage controllers for converters which are normally designed to be very fast. Hence, in secondary control and optimization design and studies, the following assumptions are usually required.

Assumption 1: The grid-forming (voltage-controlled) generators can be modeled as controllable voltage sources so that $V_i = V_i^{\mathrm{ref}}$. Therefore, considering the well-known droop equation the grid-forming units are characterized by the algebraic relationship $V_i = V_i^{\mathrm{ref}} = V_{\mathrm{nom}} - R_i^D I_i^{\mathcal{G}_e} + u_i$.

Assumption 2: The grid-following (current-/power- controlled) converters are considered as negative constant current/power loads in the ZIP load model.

In what follows, we will introduce a port-Hamiltonian (pH) representation of the system and the control by interconnection technique. Therefore, the interested readers are encouraged to refer to, e.g., [26]–[30] for more information on these concepts.

Let us define the following global matrices and vectors.

$$\begin{aligned}
\mathbf{L}_{\mathcal{G}_e} &= \mathrm{diag}\{L_i^{\mathcal{G}_e}\} \in \mathbb{R}^{n_e^{\mathcal{G}} \times n_e^{\mathcal{G}}},\\
\mathbf{R}_{\mathcal{G}_e} &= \mathrm{diag}\{R_i^{\mathcal{G}_e}\} \in \mathbb{R}^{n_e^{\mathcal{G}} \times n_e^{\mathcal{G}}},\\
\mathbf{L}_{\mathcal{E}_e} &= \mathrm{diag}\{L_j^{\mathcal{E}_e}\} \in \mathbb{R}^{n_e^{\mathcal{E}} \times n_e^{\mathcal{E}}},\\
\mathbf{R}_{\mathcal{E}_e} &= \mathrm{diag}\{R_j^{\mathcal{E}_e}\} \in \mathbb{R}^{n_e^{\mathcal{E}} \times n_e^{\mathcal{E}}},\\
\mathbf{C}_{\mathcal{N}_e} &= \mathrm{diag}\{C_k^{\mathcal{N}_e}\} \in \mathbb{R}^{n_e^{\mathcal{N}} \times n_e^{\mathcal{N}}},\\
\mathbf{P}_{\mathrm{cte}} &= \mathrm{col}\{P_k^{\mathrm{cte}}\} \in \mathbb{R}^{n_e^{\mathcal{N}}},\\
\mathbf{G}_{\mathrm{cte}} &= \mathrm{diag}\{G_k^{\mathrm{cte}}\} \in \mathbb{R}^{n_e^{\mathcal{N}} \times n_e^{\mathcal{N}}},\\
\mathbf{R}_D &= \mathrm{diag}\{R_i^D\} \in \mathbb{R}^{n_e^{\mathcal{G}} \times n_e^{\mathcal{G}}},\\
\mathbf{I}_{\mathrm{cte}} &= \mathrm{col}\{I_k^{\mathrm{cte}}\} \in \mathbb{R}^{n_e^{\mathcal{N}}},\\
\mathbf{g}_{\mathcal{N}_e}(\mathbf{q}_{\mathcal{N}_e}) &= \mathrm{diag}\{-C_k^{\mathcal{N}_e}/V_k^{\mathcal{N}_e}\} \in \mathbb{R}^{n_e^{\mathcal{N}} \times n_e^{\mathcal{N}}},\\
\mathbf{I}_{\mathcal{G}_e} &= \mathrm{col}\{I_i^{\mathcal{G}_e}\} \in \mathbb{R}^{n_e^{\mathcal{G}}},\\
\mathbf{I}_{\mathcal{E}_e} &= \mathrm{col}\{I_j^{\mathcal{E}_e}\} \in \mathbb{R}^{n_e^{\mathcal{E}}},\\
\mathbf{V}_{\mathcal{N}_e} &= \mathrm{col}\{V_k^{\mathcal{N}_e}\} \in \mathbb{R}^{n_e^{\mathcal{N}}},
\end{aligned}$$

and $\mathbf{u} = \text{col}\{u_i\} \in \mathbb{R}^{n_e^{\mathcal{G}}}$. Now, with the Hamiltonian $H(\mathbf{x}) = 0.5\mathbf{x}^\top \mathbf{Q}\mathbf{x}$ where

$$\mathbf{Q} = \begin{bmatrix} \mathbf{L}_{\mathcal{G}_e}^{-1} & \mathbf{0} & \mathbf{0} \\ \mathbf{0} & \mathbf{L}_{\mathcal{E}_e}^{-1} & \mathbf{0} \\ \mathbf{0} & \mathbf{0} & \mathbf{C}_{\mathcal{N}_e}^{-1} \end{bmatrix},$$

$$\mathbf{x} = \begin{bmatrix} \boldsymbol{\phi}_{\mathcal{G}_e} \\ \boldsymbol{\phi}_{\mathcal{E}_e} \\ \mathbf{q}_{\mathcal{N}_e} \end{bmatrix} = \mathbf{Q}^{-1} \begin{bmatrix} \mathbf{I}_{\mathcal{G}_e} \\ \mathbf{I}_{\mathcal{E}_e} \\ \mathbf{V}_{\mathcal{N}_e} \end{bmatrix},$$

one can write the system in the following form.

$$\Sigma : \begin{cases} \dot{\mathbf{x}} = \mathbf{F}\nabla H(\mathbf{x}) + \mathbf{g}_P(\mathbf{x})\mathbf{P}_{\text{cte}} + \mathbf{g}\mathbf{u} + \mathbf{E} \\ \mathbf{y} = \mathbf{g}^\top \nabla H(\mathbf{x}), \end{cases} \tag{2}$$

$$\mathbf{F} = \mathbf{J} - \mathbf{R} = \begin{bmatrix} -(\mathbf{R}_{\mathcal{G}_e} + \mathbf{R}_D) & \mathbf{0} & -\mathcal{B}_e^{\mathcal{G}\top} \\ \mathbf{0} & -\mathbf{R}_{\mathcal{E}_e} & -\mathcal{B}_e^\top \\ \mathcal{B}_e^{\mathcal{G}} & \mathcal{B}_e & -\mathbf{G}_{\text{cte}} \end{bmatrix},$$

$$\mathbf{g} = \begin{bmatrix} \mathcal{I} \\ \mathbf{0} \\ \mathbf{0} \end{bmatrix}, \quad \mathbf{g}_P(\mathbf{x}) = \begin{bmatrix} \mathbf{0} \\ \mathbf{0} \\ \mathbf{g}_{\mathcal{N}_e}(\mathbf{q}_{\mathcal{N}_e}) \end{bmatrix}, \quad \mathbf{E} = \begin{bmatrix} \mathbf{1}V_{\text{nom}} \\ \mathbf{0} \\ -\mathbf{I}_{\text{cte}} \end{bmatrix};$$

where $\mathcal{B}_e^{\mathcal{G}}$ and $\mathcal{B}_e$ are the incidence matrices defined in the preamble of this subsection; $\mathbf{J} = -\mathbf{J}^\top = 0.5[\mathbf{F} - \mathbf{F}^\top]$ and $\mathbf{R} = \mathbf{R}^\top = -0.5[\mathbf{F} + \mathbf{F}^\top]$) are the skew-symmetric and symmetric component of $\mathbf{F}$, respectively.

Assumption 3: The system Σ (2) has an equilibrium point $\bar{\mathbf{x}}$. Moreover, $\bar{\mathbf{u}}$ (resp. $\bar{\mathbf{y}}$) are the *equilibrium control* (resp. *equilibrium output*) of (2) at the equilibrium point where

$$\begin{cases} \mathbf{0} = \mathbf{F}\nabla H(\bar{\mathbf{x}}) + \mathbf{g}_P(\bar{\mathbf{x}})\mathbf{P}_{\text{cte}} + \mathbf{g}\bar{\mathbf{u}} + \mathbf{E} \\ \bar{\mathbf{y}} = \mathbf{g}^\top \nabla H(\bar{\mathbf{x}}). \end{cases}$$

The *incremental model* of the system Σ for $\tilde{\mathbf{x}} = \mathbf{x} - \bar{\mathbf{x}}$ and $\tilde{\mathbf{u}} = \mathbf{u} - \bar{\mathbf{u}}$ can then be written as the PH system below.

$$\tilde{\Sigma} : \begin{cases} \dot{\tilde{\mathbf{x}}} = [\mathbf{J} - \tilde{\mathbf{R}}(\tilde{\mathbf{x}})]\nabla H(\tilde{\mathbf{x}}) + \mathbf{g}\tilde{\mathbf{u}} \\ \tilde{\mathbf{y}} = \mathbf{g}^\top \nabla H(\tilde{\mathbf{x}}), \end{cases} \tag{3}$$

$$\tilde{\mathbf{R}}(\tilde{\mathbf{x}}) = \begin{bmatrix} \mathbf{R}_{\mathcal{G}_e} + \mathbf{R}_D & \mathbf{0} & \mathbf{0} \\ \mathbf{0} & \mathbf{R}_{\mathcal{E}_e} & \mathbf{0} \\ \mathbf{0} & \mathbf{0} & \mathbf{G}_{\text{cte}} - \mathbf{G}_P(\tilde{\mathbf{q}}_{\mathcal{N}_e}) \end{bmatrix},$$

where $\mathbf{G}_P(\tilde{\mathbf{q}}_{\mathcal{N}_e}) = \text{diag}_k\{G_k^P(\tilde{q}_k^{\mathcal{N}_e})\}$ with $G_k^P(\tilde{q}_k^{\mathcal{N}_e}) = P_k^{\text{cte}}(C_k^{\mathcal{N}_e})^2/[\bar{q}_k^{\mathcal{N}_e}(\tilde{q}_k^{\mathcal{N}_e} + \bar{q}_k^{\mathcal{N}_e})]$.

Proposition 1: With the storage function $H(\tilde{\mathbf{x}}) = 0.5\tilde{\mathbf{x}}^\top \mathbf{Q}\tilde{\mathbf{x}}$, and the passive output $\tilde{\mathbf{y}}$ with respect to $\tilde{\mathbf{u}}$, the system $\tilde{\Sigma}$ (3) is passive in the following domain.

$$\mathbb{D} = \{\tilde{\mathbf{x}} \in \mathbb{R}^{n_e^{\mathcal{G}} + n_e^{\mathcal{E}} + n_e^{\mathcal{N}}} : G_k^{\text{cte}} > \frac{P_k^{\text{cte}}(C_k^{\mathcal{N}_e})^2}{\bar{q}_k^{\mathcal{N}_e}(\tilde{q}_k^{\mathcal{N}_e} + \bar{q}_k^{\mathcal{N}_e})}\}. \tag{4}$$

Proof: Since $\mathbf{J} = -\mathbf{J}^\top$, the derivative of the storage function along the trajectories of (3) is

$$\dot{H}(\tilde{\mathbf{x}}) = -(\nabla H(\tilde{\mathbf{x}}))^\top \tilde{\mathbf{R}}(\tilde{\mathbf{x}})\nabla H(\tilde{\mathbf{x}}) + \tilde{\mathbf{y}}^\top \tilde{\mathbf{u}}. \tag{5}$$

On the other hand, the matrix $\tilde{\mathbf{R}}(\tilde{\mathbf{x}})$ is positive definite for all $\tilde{\mathbf{x}} \in \mathbb{D}$. Therefore, the system $\tilde{\Sigma}$ (3) is passive with the given storage function [30].

B. ECONOMIC DISPATCH AND NEAR-NOMINAL VOLTAGE FORMATION

Let $\mathcal{C}_i(I_i^{\mathcal{G}_e}) = \alpha_i(I_i^{\mathcal{G}_e})^2 + \beta_i(I_i^{\mathcal{G}_e}) + \gamma_i$ be ith generator cost function, where α_i, β_i, and γ_i are its parameters. If I_{demand} is the total current demand in the power network, then the economic current dispatch problem can be written as the following optimization problem.

$$\min \sum\nolimits_{i\in\mathcal{G}_e} \mathcal{C}_i(I_i^{\mathcal{G}_e}), \quad \text{s.t.} \quad \sum\nolimits_{i\in\mathcal{G}_e} I_i^{\mathcal{G}_e} = I_{\text{demand}}.$$

This optimization problem can be solved by Lagrangian method with the following Lagrangian function [31].

$$L(\mathbf{I}_{\mathcal{G}_e}, \lambda) = \sum\nolimits_{i\in\mathcal{G}_e} \mathcal{C}_i(I_i^{\mathcal{G}_e}) + \lambda(I_{\text{demand}} - \sum\nolimits_{i\in\mathcal{G}_e} I_i^{\mathcal{G}_e}),$$

where λ is *dual variable* or *Lagrange multiplier*. The primal problem is convex; hence, if Slater's condition is satisfied, then the Karush-Kuhn-Tucker (KKT) conditions provide necessary and sufficient conditions for primal-dual optimality of the points as follows [31].

$$\begin{aligned} &\text{Primal feasibility:} && \partial L/\partial\lambda = 0, \\ &\text{Stationary condition:} && \partial L/\partial I_i^{\mathcal{G}_e} = 0, \quad \forall i \in \mathcal{G}_e. \end{aligned}$$

This implies that considering a feasible equality constraint in the problem, the KKT optimality conditions are boiled down to the stationary condition [31]

$$\lim_{t\to\infty} \lambda_i = \lambda_j = \lambda_{\text{opt}} \tag{6}$$

where $\lambda_i = \partial\mathcal{C}_i/\partial I_i^{\mathcal{G}_e} = 2\alpha_i I_i^{\mathcal{G}_e} + \beta_i$ is the incremental cost (Lagrange multiplier) of ith DG, and λ_{opt} is its optimal value. This condition is known as equal incremental costs (EIC) criteria [32], [33]. Due to the fact that current sharing in power networks depends on the bus-voltage differences and not the absolute values of voltages, theoretically speaking, the above mentioned optimality condition can be satisfied in many voltage levels; i.e., λ_{opt} can have various values depending on the weighted average of voltages. However, in practice the voltages must be as close as possible to the network's nominal voltage. Therefore, the controller should also guarantee a near-nominal voltage formation which can be formulated as

$$\lim_{t\to\infty} \sum\nolimits_{i\in\mathcal{G}_e} w_i V_i = V_{\text{nom}} \sum\nolimits_{i\in\mathcal{G}_e} w_i. \tag{7}$$

where $w_i > 0, \forall i \in \mathcal{G}_e$ are the weights applied to the voltages which are defined later. We should emphasize that, following the lines of thoughts in [7], [8], [19], [22], [24], and [25] we focus on the average voltage regulation and not the containment of the voltages within limits. Therefore, we assume that the system is already designed such that, under different conditions, the steady-state voltages are within limits.

Remark 1: A special choice of the cost function parameters is $\alpha_i = 0.5/I_i^{\text{rated}}$, $\beta_i = \gamma_i = 0$ which turns (6) into the equal current ratios criteria ($I_i^{\mathcal{G}_e}/I_i^{\text{rated}} = I_j^{\mathcal{G}_e}/I_j^{\text{rated}}$) underlining the proportional current-sharing, studied in the literature (see e.g., [13]–[25]). It should be further noted that, the cost function parameters can be adjusted by upper-level strategies such as unit commitment, for different purposes.

III. CONTROLLER DESIGN, CLOSED-LOOP SYSTEM EQUILIBRIUM, AND STABILITY ANALYSIS

In this section, a distributed controller is proposed for the droop-based MG system to satisfy the control objectives in (6) and (7). The proposed controller relies on both the local and neighborhood measurements of the generators; hence, the generators need to exchange information through a communication network as described next.

A. COMMUNICATION NETWORK MODEL

A communication network between the generators can be modeled as a undirected graph with generators and communication links being its nodes and edges, respectively. Consider the graph $\mathcal{M}_c = (\mathcal{N}_c, \mathcal{E}_c, \mathcal{A})$, where $\mathcal{N}_c = \{1, \cdots, n_c^{\mathcal{N}}\}$, $\mathcal{E}_c \subseteq \mathcal{N}_c \times \mathcal{N}_c$, and $\mathcal{A} = [a_{ij}] \in \mathbb{R}^{n_c^{\mathcal{N}} \times n_c^{\mathcal{N}}}$ are its node set, edge set, and adjacency matrix, respectively. If nodes i and j exchange data, then they are neighbors, $(j, i) \in \mathcal{E}_c$, and $a_{ij} = a_{ji} > 0$; otherwise, nodes i and j are not neighbors, $(j, i) \notin \mathcal{E}_c$, and $a_{ij} = a_{ji} = 0$. Let $N_i = \{j | (j, i) \in \mathcal{E}_c\}$ and $d_i = \sum_{j \in N_i} a_{ij}$ be neighbor set and in-degree of node i, respectively. The Laplacian matrix of $\mathcal{M}_c$ is then $\mathcal{L} = \mathcal{L}^\top := \mathcal{D} - \mathcal{A}$, where $\mathcal{D} = \text{diag}\{d_i\}$ [34], [35].

B. THE DISTRIBUTED CONSENSUS-BASED CONTROL SYSTEM

The consensus algorithm [34] is an effective technique to perform a distributed solution of the KKT condition in optimization problems (the control objective (6)) [6]. Accordingly, we choose the distributed consensus-based integral controller

$$\dot{x}_i^c = k_i^I \sum\nolimits_{j \in N_i} a_{ij}(u_j^c - u_i^c), \tag{8a}$$

where u_i^c is the data shared between the DGs; x_i is the controller state; $k_i^I > 0$ is the integral gain; a_{ij} is the communication weight between DGs i and j, defined in the previous subsection. Let us define $\mathbf{x}_c = \text{col}\{x_i^c\} \in \mathbb{R}^{n_e^{\mathcal{G}}}$, $\mathbf{u}_c = \text{col}\{u_i^c\} \in \mathbb{R}^{n_e^{\mathcal{G}}}$, and $\mathbf{k}_I = \text{diag}\{k_i\} \in \mathbb{R}^{n_e^{\mathcal{G}} \times n_e^{\mathcal{G}}}$. With the Hamiltonian $H_c(\mathbf{x}_c) = 0.5\mathbf{x}_c^\top \mathbf{k}_I^{-1} \mathbf{x}_c$, this controller can then be represented as the PH system below.

$$\Sigma_c : \begin{cases} \dot{\mathbf{x}}_c = \mathbf{g}_c \mathbf{u}_c \\ \mathbf{y}_c = \mathbf{g}_c^\top \nabla H_c(\mathbf{x}_c), \end{cases} \quad \text{where } \mathbf{g}_c = -\mathbf{k}_I \mathcal{L}. \tag{8b}$$

where $\mathcal{L}$ is the Laplacian matrix of the communication network. Now if Σ_c (8b) has a feasible equilibrium point, then the incremental model of this linear system can be written as

$$\tilde{\Sigma}_c : \begin{cases} \dot{\tilde{\mathbf{x}}}_c = \mathbf{g}_c \tilde{\mathbf{u}}_c \\ \tilde{\mathbf{y}}_c = \mathbf{g}_c^\top \nabla H_c(\tilde{\mathbf{x}}_c). \end{cases} \tag{8c}$$

Therefore, one can write $\dot{H}_c(\tilde{\mathbf{x}}_c) = \tilde{\mathbf{y}}_c^\top \tilde{\mathbf{u}}_c$. Hence, with the storage function $H_c(\tilde{\mathbf{x}}_c)$, the control system $\tilde{\Sigma}_c$ (8c) is also passive (lossless) with the input $\tilde{\mathbf{u}}_c$ and output $\tilde{\mathbf{y}}_c$.

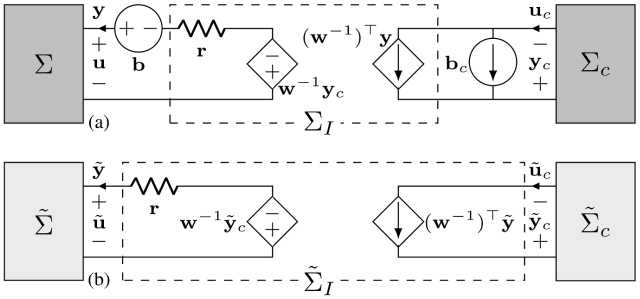

FIGURE 2. Block (circuit) diagram of the control by interconnection scheme for both non-incremental (a) and incremental (b) system models.

C. CONTROL BY INTERCONNECTION OF THE INCREMENTAL SYSTEMS

Now that the incremental model of both physical and control systems are represented as PH systems, one can couple them through the following subsystem.

$$\Sigma_I : \left\{ \begin{bmatrix} \mathbf{u} \\ \mathbf{u}_c \end{bmatrix} = \begin{bmatrix} -\mathbf{r} & -\mathbf{w}^{-1} \\ (\mathbf{w}^{-1})^\top & \mathbf{0} \end{bmatrix} \begin{bmatrix} \mathbf{y} \\ \mathbf{y}_c \end{bmatrix} + \begin{bmatrix} \mathbf{b} \\ \mathbf{b}_c \end{bmatrix}, \right. \tag{9a}$$

where $\mathbf{b} = \text{col}\{b_i\}$ and $\mathbf{b}_c = \text{col}\{b_i^c\}$ are constant vectors in $\mathbb{R}^{n_e^{\mathcal{G}}}$; $\mathbf{r}$ and $\mathbf{w}$ are square matrices belonging to $\mathbb{R}^{n_e^{\mathcal{G}} \times n_e^{\mathcal{G}}}$. We should emphasize that $\mathbf{b}$ and $\mathbf{b}_c$ do not have direct roles in the stability analysis. However, as shown in Proposition 3 in Section III-C, they are used to shape the equilibrium point of the system to comply with the control objectives.

Assumption 4: The systems Σ (2) and Σ_c (8b) have feasible equilibrium points which are coupled through the subsystem Σ_I (9a) as follows.

$$\left\{ \begin{bmatrix} \bar{\mathbf{u}} \\ \bar{\mathbf{u}}_c \end{bmatrix} = \begin{bmatrix} -\mathbf{r} & -\mathbf{w}^{-1} \\ (\mathbf{w}^{-1})^\top & \mathbf{0} \end{bmatrix} \begin{bmatrix} \bar{\mathbf{y}} \\ \bar{\mathbf{y}}_c \end{bmatrix} + \begin{bmatrix} \mathbf{b} \\ \mathbf{b}_c \end{bmatrix}. \right. \tag{9b}$$

If *Assumption 4* holds, then the incremental model of Σ_I (9a) can be written as the following lossy *interconnection subsystem* [29].

$$\tilde{\Sigma}_I : \left\{ \begin{bmatrix} \tilde{\mathbf{u}} \\ \tilde{\mathbf{u}}_c \end{bmatrix} = \begin{bmatrix} -\mathbf{r} & -\mathbf{w}^{-1} \\ (\mathbf{w}^{-1})^\top & \mathbf{0} \end{bmatrix} \begin{bmatrix} \tilde{\mathbf{y}} \\ \tilde{\mathbf{y}}_c \end{bmatrix}. \right. \tag{9c}$$

Therefore, one has

$$\tilde{\mathbf{y}}^\top \tilde{\mathbf{u}} + \tilde{\mathbf{y}}_c^\top \tilde{\mathbf{u}}_c = -\tilde{\mathbf{y}}^\top \mathbf{r} \tilde{\mathbf{y}}. \tag{9d}$$

The configuration used for control by interconnection [29] of the systems is shown in Fig. 2.

Proposition 2: Consider the PH system Σ (2) coupled with the controller Σ_c (8b) through the interconnection subsystem Σ_I (9a) (See Fig. 2). If *Assumption 4* holds and the matrix $\mathbf{R}_D + \mathbf{r}$ is positive-definite, then the equilibrium point of the closed-loop system is *asymptotically stable* in the region

$$\mathbb{S} = \{\tilde{\mathbf{x}}_t = [\tilde{\mathbf{x}}^\top, \tilde{\mathbf{x}}_c^\top]^\top : \tilde{\mathbf{x}} \in \mathbb{D}, \tilde{\mathbf{x}}_c \in \mathbb{R}^{n_e^{\mathcal{G}}}\}.$$

Proof: Consider the total storage function $H_t(\tilde{\mathbf{x}}_t) = H(\tilde{\mathbf{x}}) + H(\tilde{\mathbf{x}}_c)$ for the incremental model of the closed

loop-system which has a minimum at the equilibrium point. Taking its derivative and using (3), (8c), and (9d), one has

$$\dot{H}_t(\tilde{\mathbf{x}}_t) = \dot{H}(\tilde{\mathbf{x}}) + \dot{H}_c(\tilde{\mathbf{x}}_c) = -(\nabla H(\tilde{\mathbf{x}}))^\top \mathbf{T}(\tilde{\mathbf{x}}_t)\nabla H(\tilde{\mathbf{x}}); \tag{10}$$

$$\mathbf{T}(\tilde{\mathbf{x}}_t) = \begin{bmatrix} \mathbf{R}_{\mathcal{G}_e} + \mathbf{R}_D + \mathbf{r} & \mathbf{0} & \mathbf{0} \\ \mathbf{0} & \mathbf{R}_{\mathcal{E}_e} & \mathbf{0} \\ \mathbf{0} & \mathbf{0} & \mathbf{G}_{\text{cte}} - \mathbf{G}_P(\tilde{\mathbf{q}}_{\mathcal{N}_e}) \end{bmatrix}.$$

According to (4), $[\mathbf{G}_{\text{cte}} - \mathbf{G}_P(\tilde{\mathbf{q}}_{\mathcal{N}_e})]$ is positive-definite for all $\tilde{\mathbf{x}}_t \in \mathbb{S}$, if the closed-loop system has a feasible equilibrium point (*Assumption 4* holds). Moreover, the matrices $\mathbf{R}_{\mathcal{E}_e}$ and $\mathbf{R}_{\mathcal{G}_e}$ are also positive-definite. Therefore, if $\mathbf{R}_D + \mathbf{r}$ is positive-semi-definite, then $\mathbf{T}(\tilde{\mathbf{x}}_t)$ is positive-definite and $\dot{H}_t \leq 0, \forall \tilde{\mathbf{x}}_t \in \mathbb{S}$ which proves that the equilibrium point is *stable* in $\mathbb{S}$ [36], with Lyapunov function H_t. On the other hand, positive-definiteness of H_t ensures that $\exists \zeta > 0$ such that the level set $\Omega_\zeta = \{\tilde{\mathbf{x}}_t \in \mathbb{S} : H_t \leq \zeta\}$ is bounded. Since its requirements are all satisfied, LaSalle's theorem can be applied [36]. According to LaSalle's theorem, every solution starting in Ω_ζ converges to the largest invariant set, say $\mathbb{M}$, in $\mathbb{E} = \{\tilde{\mathbf{x}}_t \in \Omega_\zeta : \dot{H}_t = 0\}$; i.e., $\tilde{\mathbf{x}}_t \in \mathbb{M} \subseteq \mathbb{E}$ as $t \to \infty$. Since $\mathbf{T}(\tilde{\mathbf{x}}_t)$ is positive-definite $\forall \tilde{\mathbf{x}}_t \in \mathbb{S}$ and $H(\tilde{\mathbf{x}})$ is quadratic, according to (10), one can write $\mathbb{E} = \{\tilde{\mathbf{x}}_t \in \Omega_\zeta : \tilde{\mathbf{x}} = \mathbf{0}, \nabla H(\tilde{\mathbf{x}}) = \mathbf{0}\}$ implying that $\dot{\tilde{\mathbf{x}}} = \mathbf{0}$. Therefore, by using (3), (8c), and (9c) it is easy to observe that the motion in this invariant set is governed by $\dot{\tilde{\mathbf{x}}}_c = 0, \forall \mathbf{x}_t \in \mathbb{E}$. In other words, the largest invariant set in $\mathbb{E}$ is the equilibrium point; i.e., $\mathbb{M} = \{\tilde{\mathbf{x}}_t \in \Omega_\zeta : \tilde{\mathbf{x}} = \mathbf{0}, \tilde{\mathbf{x}}_c = \mathbf{0}\}$. Therefore, LaSalle's theorem implies *asymptotic stability* of the equilibrium point in $\mathbb{S}$. ■

Corollary 1: Let all the assumptions and conditions of *Propositions 1 and 2* hold. Then, if $\mathbf{P}_{\text{cte}} = \mathbf{0}$, i.e., if the constant-power loads do not exist in the system, then the equilibrium point of the closed-loop system is *globally asymptotically stable*.

Proof: According to (4), since $G_k^{\text{cte}} \geq 0$ if $P_k^{\text{cte}} = 0$ and all the conditions of *Proposition 1* hold, then one has $\mathbb{D} = \mathbb{R}^{n_e^{\mathcal{G}} + n_e^{\mathcal{E}} + n_e^{\mathcal{N}}}$ and hence $\mathbb{S} = \mathbb{R}^{2n_e^{\mathcal{G}} + n_e^{\mathcal{E}} + n_e^{\mathcal{N}}}$. Moreover, the Lyapunov function $H_t(\tilde{\mathbf{x}}_t)$ is *radially unbounded* as it is in quadratic form. Thus, the equilibrium point is *globally asymptotically stable*, if all the assumptions and conditions of *Proposition 2* hold [36]. ■

D. EQUILIBRIUM (STEADY STATE) ANALYSIS

Proposition 3: Let *Assumption 4* hold. Then, if the communication network is connected, $\mathbf{w}^{-1} = 2\boldsymbol{\alpha}$, $\mathbf{b}_c = \boldsymbol{\beta}$, and $\mathbf{b} = -k_P \mathbf{w}^{-1}\mathcal{L}\boldsymbol{\beta}$, the KKT optimality condition in (6) and the near-nominal voltage formation in (7) with $w_i = \alpha_i^{-1}$ are simultaneously achieved at the equilibrium point of the closed-loop system.

Proof: According to (8b), at equilibrium point one has $\mathcal{L}\bar{\mathbf{u}}_c = \mathbf{0}$, where we used the fact that $\mathbf{k}_I$ is positive-definite. If the communication network is connected, then $\mathcal{L}$ has a simple zero eigenvalue [34] and therefore $\bar{\mathbf{u}}_c = u_{\text{opt}}\mathbf{1}$ is the solution of $\mathcal{L}\bar{\mathbf{u}}_c = \mathbf{0}$, where u_{opt} is the consensus value. Thus, according to (9b) one can write

$$(\mathbf{w}^{-1})^\top \bar{\mathbf{y}} + \mathbf{b}_c = u_{\text{opt}}\mathbf{1}. \tag{11a}$$

Let us define $\boldsymbol{\lambda} = \text{col}\{\lambda_i\} \in \mathbb{R}^{n_e^{\mathcal{G}}}$, $\boldsymbol{\beta} = \text{col}\{\beta_i\} \in \mathbb{R}^{n_e^{\mathcal{G}}}$ and $\boldsymbol{\alpha} = \text{diag}\{\alpha_i\} \in \mathbb{R}^{n_e^{\mathcal{G}} \times n_e^{\mathcal{G}}}$. The KKT condition (6) can then be written as

$$\bar{\boldsymbol{\lambda}} = 2\boldsymbol{\alpha}\bar{\mathbf{y}} + \boldsymbol{\beta} = \lambda_{\text{opt}}\mathbf{1}. \tag{11b}$$

Therefore, if $\mathbf{w}^{-1} = 2\boldsymbol{\alpha}$ and $\mathbf{b}_c = \boldsymbol{\beta}$, then one has $u_{\text{opt}} = \lambda_{\text{opt}}$ and $\bar{\lambda}_i = \lambda_{\text{opt}}$. This underlines that the KKT condition is satisfied at the equilibrium point.

Let us further define $\mathbf{V} = \text{col}\{V_i\} \in \mathbb{R}^{n_e^{\mathcal{G}}}$. From (1e) and (9b) one can write $\bar{\mathbf{V}} = \mathbf{1}V_{\text{nom}} - \mathbf{R}_D\bar{\mathbf{y}} + \bar{\mathbf{u}}$ and $\bar{\mathbf{u}} = -\mathbf{r}\bar{\mathbf{y}} - \mathbf{w}^{-1}\bar{\mathbf{y}}_c + \mathbf{b}$, and hence $\bar{\mathbf{V}} = \mathbf{1}V_{\text{nom}} - (\mathbf{R}_D + \mathbf{r})\bar{\mathbf{y}} - \mathbf{w}^{-1}\bar{\mathbf{y}}_c + \mathbf{b}$. Multiplying this equality by $\mathbf{1}^\top\mathbf{w}$ one has

$$\mathbf{1}^\top\mathbf{w}\bar{\mathbf{V}} = \mathbf{1}^\top\mathbf{w}\mathbf{1}V_{\text{nom}} - \mathbf{1}^\top\mathbf{w}[(\mathbf{R}_D + \mathbf{r})\bar{\mathbf{y}} - \mathbf{b}] - \mathbf{1}^\top\bar{\mathbf{y}}_c.$$

Now if with $k_p \geq 0$ one selects $\mathbf{r} = -\mathbf{R}_D + k_P\mathbf{w}^{-1}\mathcal{L}\mathbf{w}^{-1}$ and $\mathbf{b} = -k_P\mathbf{w}^{-1}\mathcal{L}\boldsymbol{\beta}$, then, using (8b) and the property $\mathbf{1}^\top\mathcal{L} = \mathbf{0}^\top$ of undirected graphs [34], $\mathbf{1}^\top\mathbf{w}\bar{\mathbf{V}} = \mathbf{1}^\top\mathbf{w}\mathbf{1}V_{\text{nom}}$ can be concluded, which is equivalent to (7) with $w_i = 1/(2\alpha_i)$. ■

E. IMPLEMENTATION OF THE PROPOSED CONTROLLER

The proposed controller is presented in matrix form so far. However, in what follows, to better understand its practical implementation, it is formulated in a non-matrix format in terms of the required measurements, parameters, and communication data. If $\mathbf{w} = 0.5\boldsymbol{\alpha}^{-1}$, $\mathbf{r} = -\mathbf{R}_D + k_P 2\boldsymbol{\alpha}\mathcal{L}2\boldsymbol{\alpha}$, $\mathbf{b}_c = \boldsymbol{\beta}$, and $\mathbf{b} = -k_P 2\boldsymbol{\alpha}\mathcal{L}\boldsymbol{\beta}$, then considering (2) and defining $\mathbf{z}_\lambda = \text{col}\{z_i^\lambda\} = -\mathcal{L}\boldsymbol{\lambda}$, and $\mathbf{z}_c = \text{col}\{z_i^c\} = -\mathcal{L}\mathbf{x}_c$, the control system (8b) coupled with the interconnection subsystem (9a) can be written as

$$\mathbf{u} = \mathbf{R}_D\mathbf{I}_{\mathcal{G}_e} + 2\boldsymbol{\alpha}(k_P\mathbf{z}_\lambda - \mathbf{z}_c), \quad \dot{\mathbf{x}}_c = \mathbf{k}_I\mathbf{z}_\lambda,$$

which can be written in the following scalar format.

$$\begin{cases} u_i = R_i^D I_i^{\mathcal{G}_e} + 2\alpha_i(k_P z_i^\lambda - z_i^c) \\ \dot{x}_i^c = k_i^I z_i^\lambda \\ z_i^\lambda = \sum_{j\in N_i} a_{ij}(\lambda_j - \lambda_i) \\ z_i^c = \sum_{j\in N_i} a_{ij}(x_j^c - x_i^c) \\ \lambda_i = 2\alpha_i I_i^{\mathcal{G}_e} + \beta_i. \end{cases} \tag{12}$$

Fig. 3 depicts a schematic diagram of the proposed controller described in (12). One can see that except for x_j^c and λ_j, received from the neighboring DGs, the other parameters and variables are locally available for each DG.

IV. CASE STUDIES AND RESULTS

To show the effectiveness of the proposed controller, it is tested on a 48-Volt meshed dc MG, powered by six DGs. The DGs with odd (resp. even) numbers are interfaced to the grid via buck (resp. boost) converters, which are depicted in

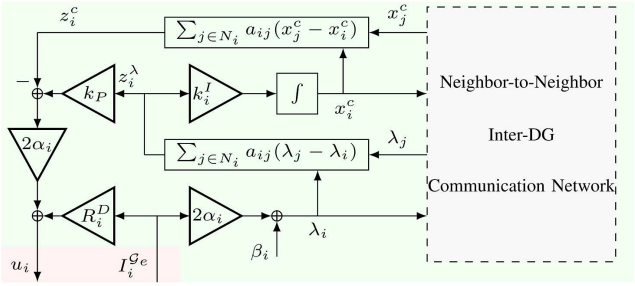

FIGURE 3. Schematic diagram of the proposed distributed controller.

TABLE 1. The electrical and control specifications of the test MG.

DGs' Specifications with Base RL of $(0.15\Omega, 300\mu H)$						
	DG Number ($i \in \mathcal{G}_e$)					
	1	2	3	4	5	6
$I_i^{\text{rated}}(A)$	12	4	8	8	6	5
$R_i^D(V/A)$	0.2	0.6	0.3	0.3	0.4	0.48
$\alpha_i(10^{-1}\$/A^2)$	0.8	1.9	1	1.4	1.2	1.6
$\beta_i(10^{-2}\$/A)$	1	2.5	1.2	1.8	1.5	2.1
$\gamma_i(10^{-1}\$)$	2	5	2	4	3	4
$R_i^{\mathcal{G}_e}, L_i^{\mathcal{G}_e}$ (p.u.)	0.5	0.4	0.55	0.6	0.45	0.5
k_i^P	5					
k_i^I	100 or 400					

Line Specifications ($R_i^{\mathcal{E}_e}, L_i^{\mathcal{E}_e}$) with Base RL of $(0.15\Omega, 300\mu H)$								
	Line Number ($j \in \mathcal{E}_e$)							
	1	2	3	4	5	6	7	8
(p.u.)	1	2	2	1	1	3	1	2

Bus Specifications								
	Bus Number ($k \in \mathcal{N}_e$)							
	1	2	3	4	5	6	7	8
$C_k^{\mathcal{N}_e}(F)$	22×10^{-3}							
$1/G_k^{\text{cte}}(\Omega)$	40	30	30	30	40	30	20	25
$I_k^{\text{cte}}(A)$	1	1.2	0.8	1	0.9	1	0.9	0.8
$P_k^{\text{cte}}(W)$	$0.8G_k^{\text{cte}}V_n^2$ where $V_n = 48V$							

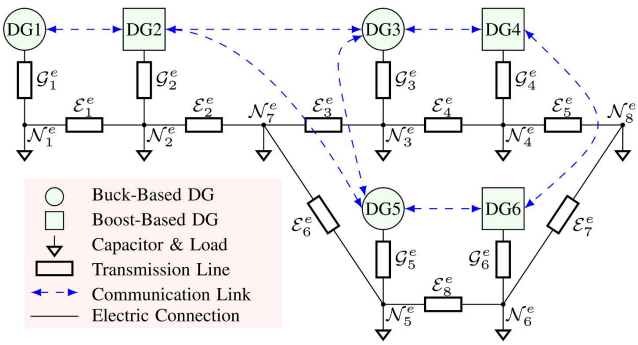

FIGURE 4. Electrical and communication networks of the test microgrid system.

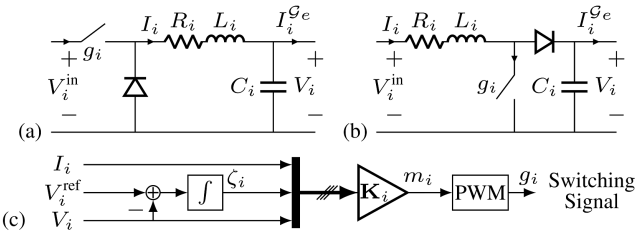

FIGURE 5. Converter circuit dynamics and internal controller; (a) buck converter, (b) boost converter, and (c) LQR-based voltage controller.

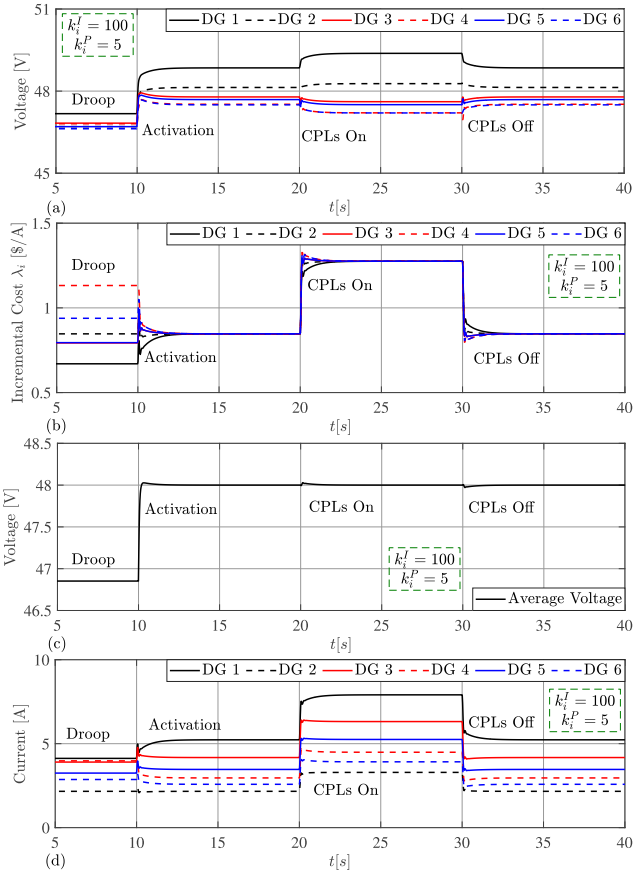

FIGURE 6. Case Study 1: Activation and load change; (a) voltages, (b) incremental costs, (c) weighted average of the voltages, and (d) currents.

Fig. 4 by circles (resp. squares). The electrical and control specifications of the MG shown in Fig. 4 are given in Table 1.

Remark 2: According to Assumption 1, to design the secondary controller, the converters are modeled by an equivalent zero-order model as in (1e); thus, the converter dynamics and its internal voltage controller are hidden in Fig. 1 under the dashed blue box. However, in the simulations, Linear Quadratic Regulator (LQR) controller technique is used for the voltage V_i to track its reference V_i^{ref} [37]. Fig. 5 depicts the converter dynamics and the internal voltage controller. The resistance R_i, inductance L_i, and capacitance C_i of all the converters are 0.1Ω, $2.64mH$, and $2.2mF$, respectively; the input voltage to the converters V_i^{in} of the DGs 1 to 6 are 80, 25, 100, 20, 80, 25 V, respectively; I_i, ζ_i, and V_i are the states of the system, m_i is the duty cycle given to the PWM generator to produce the switching signal g_i with frequency of 5kHz. To design proper feedback gain matrix $\mathbf{K}_i \in \mathbb{R}^{3\times 3}$, the linearized second-order average model of converters augmented with a voltage-tracker integrator, is used where the output current of the converter capacitor $I_i^{\mathcal{G}_e}$ is considered as an external disturbance, along the lines of [37].

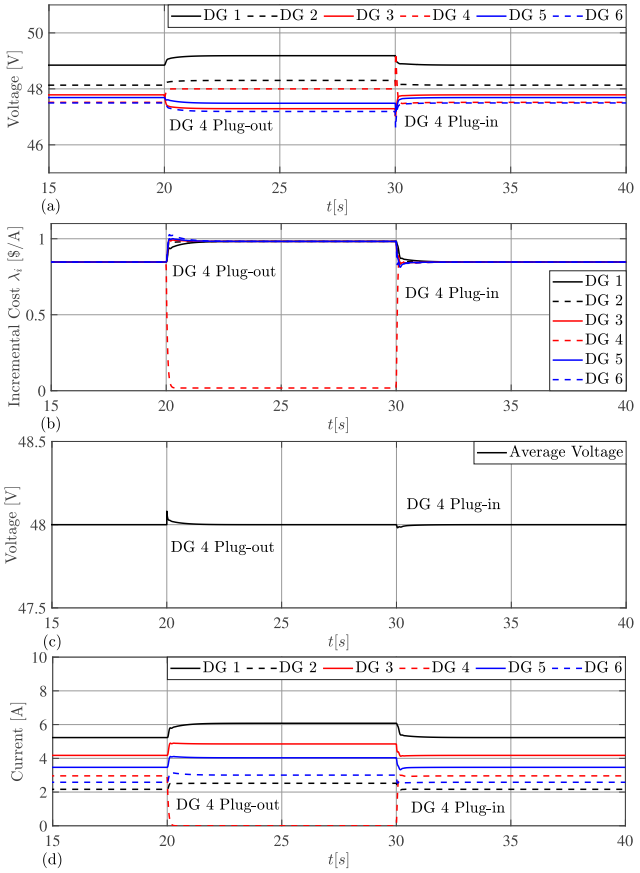

FIGURE 7. Case Study 2: DG Disconnection/connection; (a) voltages, (b) incremental costs, (c) weighted average of the voltages, and (d) currents.

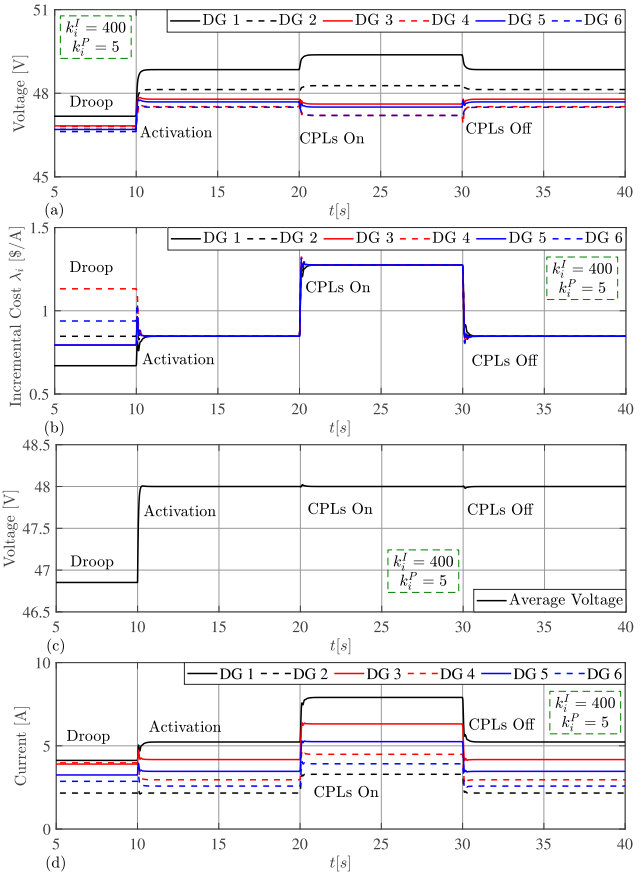

FIGURE 8. Case Study 3: Impact of integral gain on convergence speed; (a) voltages, (b) incremental costs, (c) weighted average of the voltages, and (d) currents.

A. CASE STUDY 1: ACTIVATION AND LOAD CHANGE

Fig. 6 depicts the performance of the MG under the proposed controller in different stages. Before $t = 10s$, the MG is operated without the proposed secondary control. Therefore, the DGs voltages are settled away from their nominal voltages so that their average value is deviated from the nominal value $48V$. Moreover, the incremental costs of the DGs have different values which underlines the KKT condition is not satisfied. After activating the controller at $t = 10s$, the DGs reach a consensus on their incremental costs and at the same time they form their voltages around the nominal value with a weighted average of nominal voltage. It should be noted that before $t = 20s$, only constant impedance and constant current loads are energized. To emphasis the resiliency of the controller, at $t = 20s$, the constant power loads (CPLs) at all the buses are activated. One can see that the DGs reach an agreement on a new optimal incremental cost higher than the previous one, which returns to the previous value after deactivating the constant power loads at $t = 30s$. It should be emphasized that, over the load change transitions, the average voltage remains unchanged and only transient voltage drifts from the nominal voltage are observed.

B. CASE STUDY 2: DG DISCONNECTION/CONNECTION (PLUG-AND-PLAY)

The results for this case are given in Fig. 7. To show the DGs plug-and-play ability under the proposed controller, the 4th DG is disconnected from the grid at $t = 20s$ and it is connected back to the grid at $t = 30s$. To do so, a corresponding circuit breaker is opened at $t = 20s$ to disconnect the DG physically and the communication links related to the DG are all interrupted. Moreover, before closing the breaker at $t = 30s$, all the communication links are restored and both sides of the breaker are voltage-synchronized for seamless connection of the DG. According to Fig. 7, after disconnecting 4th DG from the grid, other DGs inject more current so they reach consensus on a new optimal incremental cost. Furthermore, one can see that the average voltage of the remaining five DGs still operate at the nominal value. It is also shown that after connecting it back to the grid, the DG immediately participates in the current sharing and voltage formation tasks as before.

C. CASE STUDY 3: IMPACT OF INTEGRAL GAIN ON CONVERGENCE SPEED

Fig. 8 shows the responses of the DGs under the proposed controller for an integral gain of $k_i^I = 400$ which is 4 times

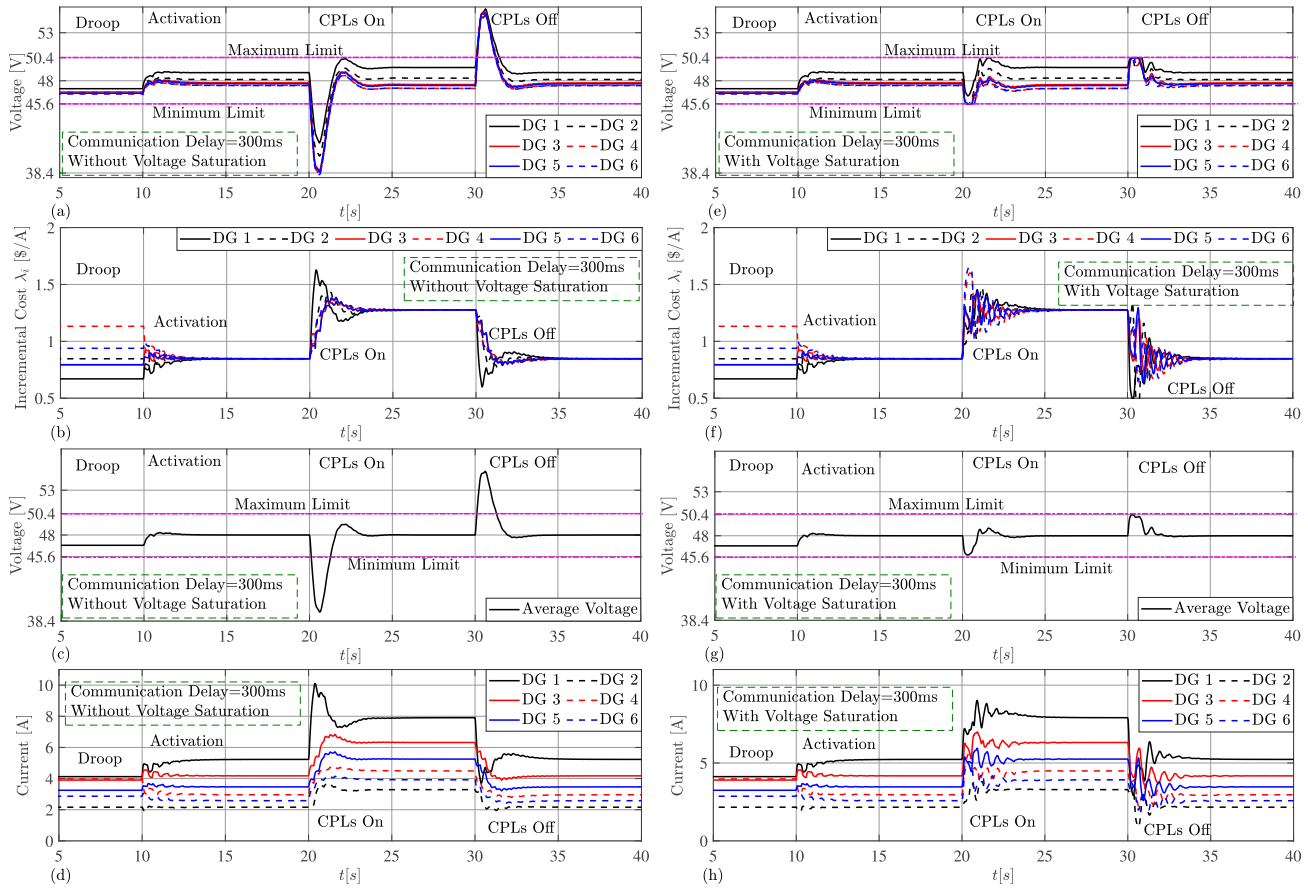

FIGURE 9. Case Study 4: Impacts of communication delay and voltage limitation; (a) and (e) voltages, (b) and (f) incremental costs, (c) and (g) weighted average of the voltages, and (d) and (h) currents. First column represents the DG responses without applying the voltage reference saturation. The second column represents the responses under the saturation of the voltage references.

the gain used in the first case study. Case studies 1 and 3 are similar. Comparing Fig. 6 and Fig. 8, we can see that the convergence speed and system performance can be adjusted by the integral control gain.

D. CASE STUDY 4: IMPACTS OF COMMUNICATION DELAY AND VOLTAGE LIMITATION

In this subsection, we re-simulated Case Study 1 with the same parameters, but in the presence of a communication delay of 300ms. Moreover, we also included these results when pre-specified voltage limits are considered, to investigate its applicability under voltage saturation constraints. According to Fig. 9 (a)-(d), when the converter voltage references V_i^{ref} are not saturated, the communication delay causes so severe oscillations that the voltages go beyond the limits after load changes at $t = 20s$ and $t = 30s$. However, considering the limitation of the voltages and saturation of V_i^{ref}, from Fig. 9 (e)-(h), we can see that the voltages can stay within limits after these events and that the oscillations are transmitted to the currents and hence the incremental costs. Generally, we can say the communication delays can cause oscillation in the system responses and prolong the settling (convergence) time. The magnitude of the oscillations and duration of the convergence can vary depending on the values of the delay duration and control gains. In this paper, we did not perform theoretical time-delay analysis, as it is out of scope of this work; however, it can be considered in future researches. But, generally speaking, faster systems with larger integral gains are expected to be more vulnerable to communication delays. The interested readers can get more info on the impacts of delay on the system stability and performance in [38].

E. CASE STUDY 5: IMPACT OF COMMUNICATION LINK INTERRUPTION

In this section we repeat the scenario in Case Study 3, but considering the interruption of some of the communication links. We assume that the controller is activated at $t = 10s$, and the CPLs are turned on and off at $t = 20s$ and $t = 30s$, respectively. We also assume that the 5th DG loses its communication channels with the 2nd and 3rd DGs at $t = 15s$, and these channels are recovered at $t = 35s$. According to Fig. 10, after interrupting the communication links, since the remaining communication network is still connected, the controller can recover the voltages and the currents after a short transient. Moreover, comparing Figs 8 and 10, we can

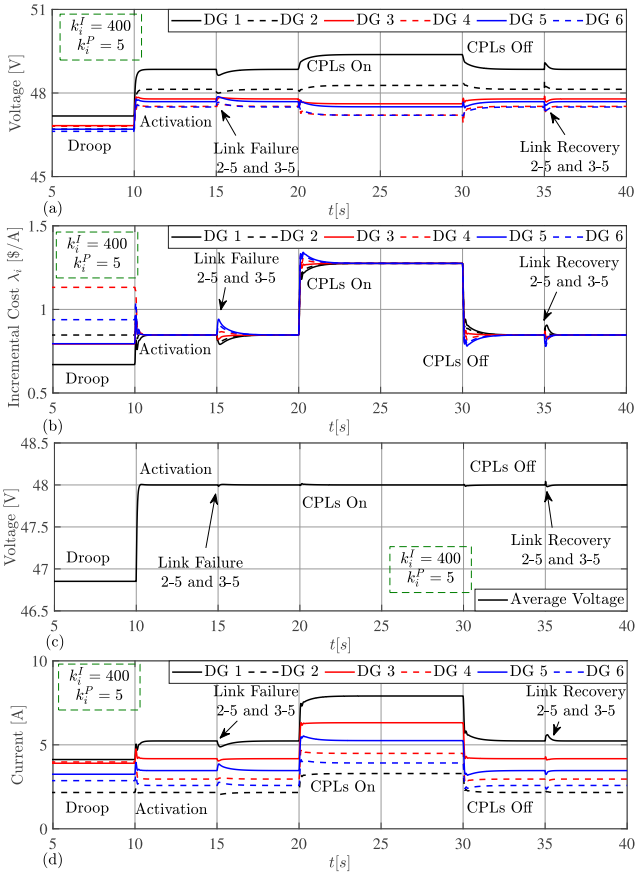

FIGURE 10. Case Study 5: Impact of communication link interruption; (a) voltages, (b) incremental costs, (c) weighted average of the voltages, and (d) currents.

see that under the new network without the interrupted links, the load-change transient response of the system is a bit slower. This is due to the lower connectivity of the remaining communication graph which has an important role in the convergence speed. At $t = 35s$, we recover the lost communication links. The simulation results show that the controller is resilient against the communication link interruption, as long as the remaining network is connected, i.e., as long as the conditions of Propositions 2 and 3 are satisfied.

F. CASE STUDY 6: REAL-TIME RESULTS FROM OPAL-RT

To verify the real-time effectiveness of the proposed controller, the previous system is built and loaded to an OPAL-RT OP5600 real-time simulator, shown in Fig. 11. It should be pointed out that, therein, the detailed switching model of the Buck and Boost converters with switching frequency of 5kHz are employed. The selected IGBTs and Diodes have internal resistance of $1m\Omega$ and forward voltage of $0.8V$. The other (passive) components of the converters and their inner voltage controllers are exactly the same as described in the preamble of this Section (Remark 2).

Fig. 12 indicates alignment of the real-time system responses with the simulation results in Section IV-A. Due to the input limitation of the oscilloscope only the results for the DGs 1, 2, 5, and 6 are given. After activating the controller,

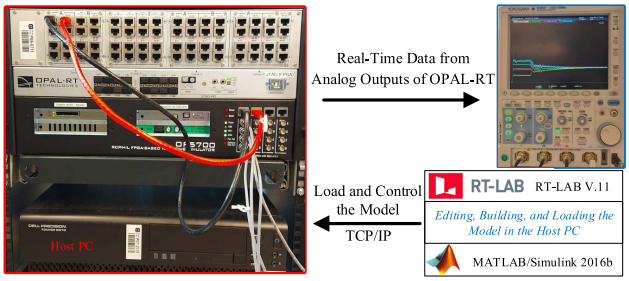

FIGURE 11. Real-time simulation setup.

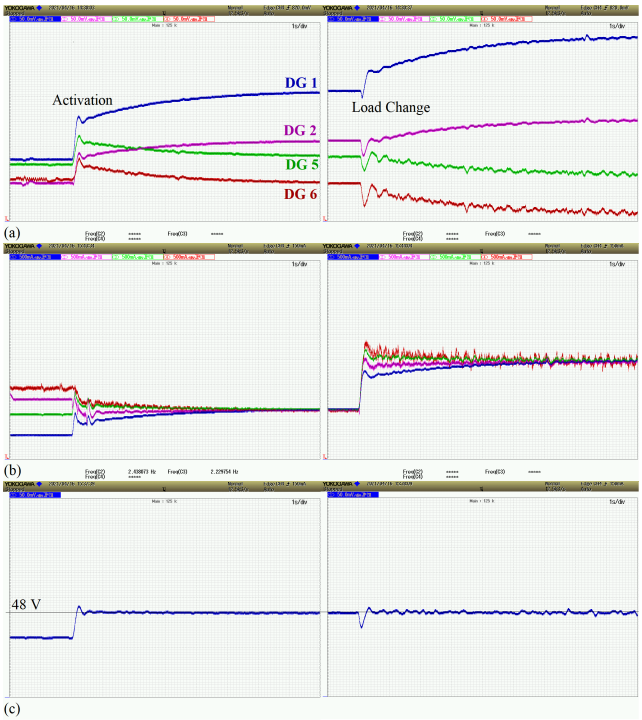

FIGURE 12. Case Study 6: Real-time results; (a) the voltages, (b) the incremental costs, and (c) weighted average of the voltages.

the incremental costs reach a consensus and the voltages reach a formation around the nominal value so that their weighted average settles at the nominal value. The results for the load increase scenario further approves the effectiveness of the proposed control in reaching the current-sharing and voltage-formation control goals, under severe load changes.

G. CASE STUDY 7: COMPARISON WITH THE EXISTING METHODS

In this subsection, we include the system responses under different control methods existing in the literature. To have a fair comparison, according to Remark 1, we have considered the proportional current-sharing problem, as a common ground. Moreover, the control parameters are tuned in a way that the system has somewhat similar transient response and settling time, under these different methods. It is assumed that the communication delay is $10ms$. According to Fig. 13, we can see that, unlike the other methods, the compromised control technique in [14] does not provide accurate current-sharing among all the the DGs, as the 1st DG is selected as the leader

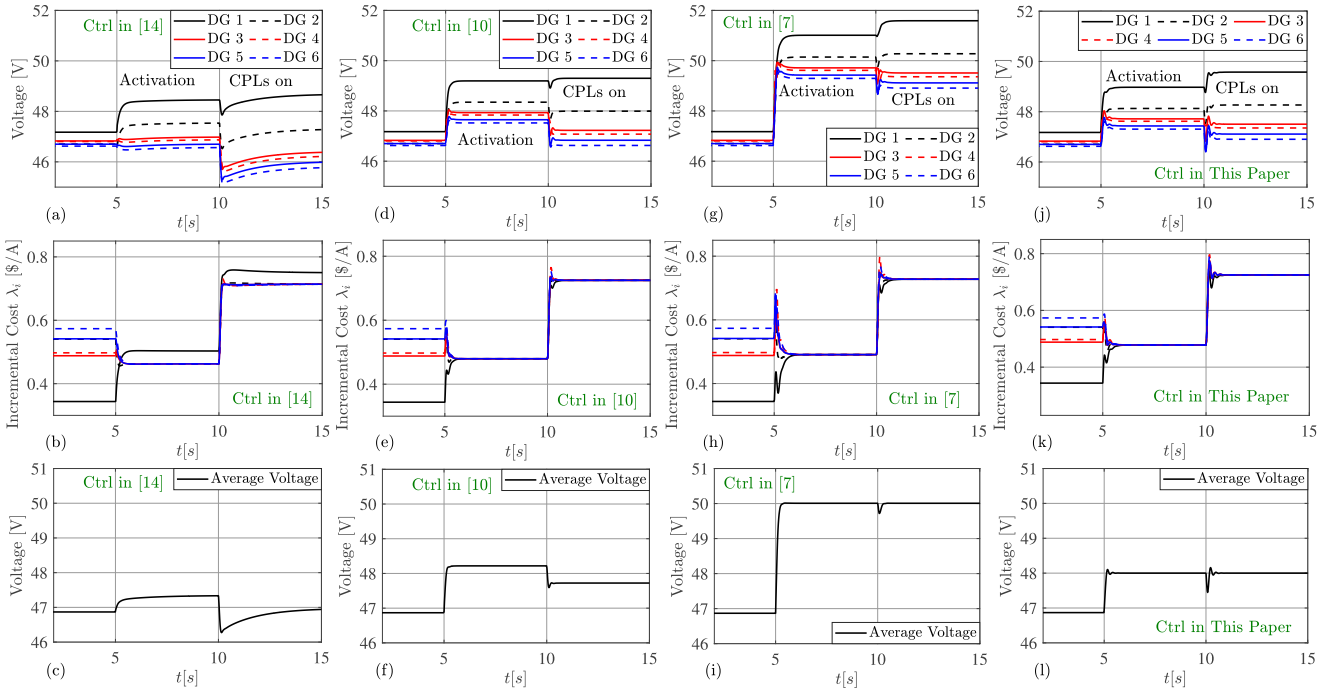

FIGURE 13. Case Study 7: Comparison with the existing methods. Figures in the first, second, and third rows show the voltages, incremental costs, and weighted average of the voltages, respectively. Figures in the first, second, third, and forth columns show the responses under the control methods in [7], [10], [14], and this paper, respectively.

DG due to its highest current capacity. Another observation is that, despite providing accurate current-sharing, compared to our propose controller, the methods in [7] and [10] do not provide accurate average voltage regulation. It should be further noted that in our simulations, we observed that the deviation of the average voltage from the nominal value, under the methods in [7] and [10], highly depends on the initial conditions and communication delay. However, as shown in Case Study 4, the proposed controller in this paper can successfully provide accurate current-sharing and average voltage regulation even in the presence of the communication delay of 300ms.

V. CONCLUSION

A distributed secondary control technique is proposed for dc MGs with ZIP loads which drives the MG to a point where the KKT optimality condition is satisfied for all the DGs and their weighted-average voltage is the nominal value. The closed-loop system (the MG engaged with the proposed controller) is formulated in a port-Hamiltonian representation which is shown to be asymptotically stable by using Lyapunov and LaSalle theorems. It is also shown that the system is globally asymptotically stable without the constant power loads. The effectiveness of the proposed controller for different case studies is verified by adapting it to a test system through both non-real-time and real-time simulations. It should be noted that for the theoretical analyses each DG is modeled by an equivalent zero order model as a controllable voltage source, while, in MATLAB/Simulink simulation and OPAL-RT model the average model and detailed switching model are used, respectively. All in all, the theoretical analyses and case studies demonstrate effectiveness of the proposed controller in achieving the desired control goals.

Some additional research directions are to consider the discrete models of the system and communication delays and/or the output and input constraints to increase the practicality and robustness of the system. These latter issues have been discussed in the recent studies by the researchers in the control and cybernetic engineering communities, for example, [39], [40]. Utilizing such intelligent algorithms to improve robustness and handle more complicated input constraints can be considered a potential future work. Another interesting topic is to study the influences of signal switching and state discontinuity during the control process.

ACKNOWLEDGMENT

The authors would like to thank Prabhat Ranjan Bana for his help in obtaining the real-time results from OPAL-RT.

REFERENCES

[1] N. Hatziargyriou, H. Asano, R. Iravani, and C. Marnay, "Microgrids," *IEEE Power Energy Mag.*, vol. 5, no. 4, pp. 78–94, Jul./Aug. 2007.
[2] B. Abdolmaleki, Q. Shafiee, M. M. Arefi, and T. Dragicevic, "An instantaneous event-triggered Hz–Watt control for microgrids," *IEEE Trans. Power Syst.*, vol. 34, no. 5, pp. 3616–3625, Sep. 2019.
[3] L. Meng, Q. Shafiee, G. F. Trecate, H. Karimi, D. Fulwani, X. Lu, and J. M. Guerrero, "Review on control of DC microgrids and multiple microgrid clusters," *IEEE J. Emerg. Sel. Topics Power Electron.*, vol. 5, no. 3, pp. 928–948, Sep. 2017.
[4] C. Albea-Sánchez, "Hybrid dynamical control based on consensus algorithms for current sharing in DC-bus microgrids," *Nonlinear Anal., Hybrid Syst.*, vol. 39, Feb. 2021, Art. no. 100972.
[5] Y. Han, X. Ning, P. Yang, and L. Xu, "Review of power sharing, voltage restoration and stabilization techniques in hierarchical controlled DC microgrids," *IEEE Access*, vol. 7, pp. 149202–149223, 2019.

[6] D. K. Molzahn, F. Dörfler, H. Sandberg, S. H. Low, S. Chakrabarti, R. Baldick, and J. Lavaei, "A survey of distributed optimization and control algorithms for electric power systems," *IEEE Trans. Smart Grid*, vol. 8, no. 6, pp. 2941–2962, Nov. 2017.

[7] V. Nasirian, S. Moayedi, A. Davoudi, and F. L. Lewis, "Distributed cooperative control of dc microgrids," *IEEE Trans. Power Electron.*, vol. 30, no. 4, pp. 2288–2303, Apr. 2015.

[8] S. Sahoo and S. Mishra, "An adaptive event-triggered communication-based distributed secondary control for DC microgrids," *IEEE Trans. Smart Grid*, vol. 9, no. 6, pp. 6674–6683, Nov. 2018.

[9] S. Sahoo and S. Mishra, "A distributed finite-time secondary average voltage regulation and current sharing controller for DC microgrids," *IEEE Trans. Smart Grid*, vol. 10, no. 1, pp. 282–292, Jan. 2019.

[10] B. Abdolmaleki, Q. Shafiee, M. S. Sadabadi, and T. Dragicevic, "Economical secondary control of DC microgrids," in *Proc. IEEE 11th Int. Symp. Power Electron. Distrib. Gener. Syst. (PEDG)*, Dubrovnik, Croatia, Sep. 2020, pp. 304–308.

[11] J. Peng, B. Fan, and W. Liu, "Voltage-based distributed optimal control for generation cost minimization and bounded bus voltage regulation in DC microgrids," *IEEE Trans. Smart Grid*, vol. 12, no. 1, pp. 106–116, Jan. 2021.

[12] J. Peng, B. Fan, Q. Yang, and W. Liu, "Distributed event-triggered control of DC microgrids," *IEEE Syst. J.*, vol. 15, no. 2, pp. 2504–2514, Jun. 2021.

[13] R. Han, L. Meng, J. M. Guerrero, and J. C. Vasquez, "Distributed nonlinear control with event-triggered communication to achieve current-sharing and voltage regulation in DC microgrids," *IEEE Trans. Power Electron.*, vol. 33, no. 7, pp. 6416–6433, Jul. 2018.

[14] R. Han, H. Wang, Z. Jin, L. Meng, and J. M. Guerrero, "Compromised controller design for current sharing and voltage regulation in DC microgrid," *IEEE Trans. Power Electron.*, vol. 34, no. 8, pp. 8045–8061, Aug. 2019.

[15] S. Sahoo, D. Pullaguram, S. Mishra, J. Wu, and N. Senroy, "A containment based distributed finite-time controller for bounded voltage regulation & proportionate current sharing in DC microgrids," *Appl. Energy*, vol. 228, pp. 2526–2538, Oct. 2018.

[16] M. Cucuzzella, S. Trip, and J. Scherpen, "A consensus-based controller for DC power networks," *IFAC-PapersOnLine*, vol. 51, no. 33, pp. 205–210, 2018.

[17] M. Cucuzzella, K. C. Kosaraju, and J. M. A. Scherpen, "Distributed passivity-based control of DC microgrids," in *Proc. Amer. Control Conf. (ACC)*, Philadelphia, PA, USA, Jul. 2019, pp. 652–657.

[18] S. Trip, R. Han, M. Cucuzzella, X. Cheng, J. Scherpen, and J. Guerrero, "Distributed averaging control for voltage regulation and current sharing in DC microgrids: Modelling and experimental validation," *IFAC-PapersOnLine*, vol. 51, no. 23, pp. 242–247, 2018.

[19] S. Trip, M. Cucuzzella, X. Cheng, and J. Scherpen, "Distributed averaging control for voltage regulation and current sharing in DC microgrids," *IEEE Control Syst. Lett.*, vol. 3, no. 1, pp. 174–179, Jan. 2019.

[20] A. Silani, M. Cucuzzella, J. M. A. Scherpen, and M. J. Yazdanpanah, "Passivity properties for regulation of DC networks with stochastic load demand," *IFAC-PapersOnLine*, vol. 53, no. 2, pp. 13113–13118, 2020.

[21] S. Trip, M. Cucuzzella, C. De Persis, X. Cheng, and A. Ferrara, "Sliding modes for voltage regulation and current sharing in DC microgrids," in *Proc. Annu. Amer. Control Conf. (ACC)*, Milwaukee, WI, USA, Jun. 2018, pp. 6778–6783.

[22] M. Cucuzzella, S. Trip, C. De Persis, X. Cheng, A. Ferrara, and A. van der Schaft, "A robust consensus algorithm for current sharing and voltage regulation in DC microgrids," *IEEE Trans. Control Syst. Technol.*, vol. 27, no. 4, pp. 1583–1595, Jul. 2019.

[23] P. Nahata and G. Ferrari-Trecate, "On existence of equilibria, voltage balancing, and current sharing in consensus-based DC microgrids," in *Proc. Eur. Control Conf. (ECC)*, St. Petersburg, Russia, May 2020, pp. 1216–1223.

[24] P. Nahata, M. S. Turan, and G. Ferrari-Trecate, "Consensus-based current sharing and voltage balancing in DC microgrids with exponential loads," *IEEE Trans. Control Syst. Technol.*, early access, Nov. 10, 2021, doi: 10.1109/TCST.2021.3120321.

[25] M. S. Sadabadi, "A distributed control strategy for parallel DC-DC converters," *IEEE Control Syst. Lett.*, vol. 5, no. 4, pp. 1231–1236, Oct. 2021.

[26] A. Van Der Schaft and D. Jeltsema, *Port-Hamiltonian Systems Theory: An Introductory Overview*. Boston, MA, USA: Now Foundations and Trends, 2014.

[27] B. Fu, S. Li, X. Wang, and L. Guo, "Output feedback based simultaneous stabilization of two port-controlled Hamiltonian systems with disturbances," *J. Franklin Inst.*, vol. 356, no. 15, pp. 8154–8166, Oct. 2019.

[28] B. Fu, X. Wang, and Q. Wang, "Protocol design for group output consensus of disturbed port-controlled Hamiltonian multi-agent systems," *J. Franklin Inst.*, vol. 358, no. 18, pp. 9867–9889, Dec. 2021.

[29] R. Ortega, A. V. D. Schaft, F. Castanos, and A. Astolfi, "Control by interconnection and standard passivity-based control of port-Hamiltonian systems," *IEEE Trans. Autom. Control*, vol. 53, no. 11, pp. 2527–2542, Dec. 2008.

[30] R. Ortega, A. J. Van der Schaft, I. Mareels, and B. Maschke, "Putting energy back in control," *IEEE Control Syst. Mag*, vol. 21, no. 2, pp. 18–33, Apr. 2001.

[31] S. Boyd and L. Vandenberghe, *Convex Optimization*. Cambridge, MA, USA: Cambridge Univ. Press, 2004.

[32] B. Abdolmaleki and Q. Shafiee, "Online Kron reduction for economical frequency control of microgrids," *IEEE Trans. Ind. Electron.*, vol. 67, no. 10, pp. 8461–8471, Oct. 2020.

[33] A. J. Wood, B. F. Wollenberg, and G. B. Sheblé, *Power Generation, Operation, and Control*, 3rd ed. Hoboken, NJ, USA: Wiley, 2013.

[34] R. Olfati-Saber, J. A. Fax, and R. M. Murray, "Consensus and cooperation in networked multi-agent systems," *Proc. IEEE*, vol. 95, no. 1, pp. 215–233, Jan. 2007.

[35] B. Abdolmaleki, Q. Shafiee, A. R. Seifi, M. M. Arefi, and F. Blaabjerg, "A zeno-free event-triggered secondary control for AC microgrids," *IEEE Trans. Smart Grid*, vol. 11, no. 3, pp. 1905–1916, May 2020.

[36] H. K. Khalil, *Nonlinear Systems*, 3rd ed. Englewood Cliffs, NJ, USA: Prentice-Hall, 2002.

[37] M. S. Sadabadi, Q. Shafiee, and A. Karimi, "Plug- and-play robust voltage control of DC microgrids," *IEEE Trans. Smart Grid*, vol. 9, no. 6, pp. 6886–6896, Nov. 2018.

[38] E. Fridman, *Introduction to Time-Delay Systems: Analysis and Control*. Basel, Switzerland: Birkhäuser, 2014.

[39] T. Yang, N. Sun, and Y. Fang, "Adaptive fuzzy control for a class of MIMO underactuated systems with plant uncertainties and actuator deadzones: Design and experiments," *IEEE Trans. Cybern.*, early access, Feb. 2, 2021, doi: 10.1109/TCYB.2021.3050475.

[40] T. Yang, N. Sun, and Y. Fang, "Neuroadaptive control for complicated underactuated systems with simultaneous output and velocity constraints exerted on both actuated and unactuated states," *IEEE Trans. Neural Netw. Learn. Syst.*, early access, Oct. 8, 2021, doi: 10.1109/TNNLS.2021.3115960.

BABAK ABDOLMALEKI (Member, IEEE) is currently pursuing the Ph.D. degree with the Department of Electric Power Engineering, Norwegian University of Science and Technology (NTNU), Trondheim, Norway. His research interests include numerical simulations, feedback control, and optimization of dynamical systems applied to power electronics and power systems.

GILBERT BERGNA-DIAZ (Member, IEEE) received the degree in electrical power engineering from the Universidad Simón Bolívar, Caracas, Venezuela, in 2008, the research master's degree in electrical energy from the École Supérieure dÉlectricité (Supélec), Paris, France, in 2010, and the joint Ph.D. degree in electric power engineering from the École Centrale Supélec, Paris, and the Norwegian University of Science and Technology (NTNU), Trondheim, Norway, in 2015. In 2014, he joined SINTEF Energy Research as a Research Scientist, where he was involved in modelling, analysis, and control of HVdc transmission systems. In 2016, he joined the Department of Electric Power Engineering, NTNU, as a Post-Doctoral Research Fellow, where he was involved in energy-based modeling and nonlinear control of multiterminal HVdc grids. Since 2019, he has been an Associate Professor with the Department of Electric Power Engineering.